Ángel J. Molina-Viedma, Luis Felipe-Sesé, Elías López-Alba, Francisco A. Díaz, Thermoelastic effect in modal shapes at high frequencies using infrared thermography, Measurement, Volume 176, 2021, 109180, ISSN 0263-2241, https://doi.org/10.1016/j.measurement.2021.109180.

Thermoelastic effect in modal shapes at high frequencies using infrared thermography

Ángel J. Molina-Viedma*[1], Luis Felipe-Sesé[1], Elías López-Alba[2], Francisco A. Díaz[2]

[1]Departamento de Ingeniería Mecánica y Minera, Campus Científico Tecnológico de Linares, Universidad de Jaén, 23700 Linares, Spain

[2]Departamento de Ingeniería Mecánica y Minera, Campus Las Lagunillas, Universidad de Jaén, 23071 Jaén, Spain

*Corresponding author: ajmolina@ujaen.es

Abstract

Infrared thermography is employed by different methodologies and techniques to perform characterisations and evaluations in solids, typically related to fracture mechanics and damage, based on monitoring heat generation or temperature changes. In this study, the limits of the current technology for Thermoelastic Stress Analysis (TSA), usually employed under low-frequency loads, are explored to characterise temperature fields associated to the first stress invariant in mode shapes. Higher frequencies are especially emphasised in this research. Eleven modes of a plate were analysed, reaching frequencies over 2 000 Hz. High correlation coefficients were obtained in comparison with the first stress invariant fields of a finite element model, with a detriment as the mode's order increases. In those cases, this study highlights the combined influence of the specimen response and mode shape stiffness as well as the progressively shorter integration time.

Keywords: Thermoelasticity; modal analysis; infrared thermography; high frequency

1. Introduction

Infrared radiation (IR) is inherent to any object whose temperature is above absolute zero. Its emittance is proportional to the temperature raised to the forth power. With the recent developments in IR cameras technology, thermography arises as a powerful tool for many applications in scientific research and industry that exploits the temperature fields for the study or identification of multiple phenomena. From the mechanical point of view, elements subjected to loads suffer temperature variations due to internal thermal processes. Many methodologies and techniques analyse the infrared emission for different properties characterisation or detection and location of damage. Both metals and non-metals materials, such as polymers or composites, take advantage of the versatility.

In non-destructive testing, the methodologies are based on active or pasive thermography, depending on whether an external stimulation is required or not, respectively, to generate heat [1,2]. Additionally, one of the most relevant applications of thermography is for Thermoelastic Stress Analysis (TSA) [3,4]. This technique is based on the direct relation between the first stress invariant (sum of the normal stresses) and a quick heat generation in adiabatic conditions. Most of the work using this methodology has entailed the study of fracture and fatigue phenomena [5,6]. The most employed methodologies evaluate the periodic variation of temperature performing a monotonic cycling excitation and a lock-in strategy to extract the temperature oscillation at the loading frequency. Lock-in has been usually performed by hardware using an amplifier, but can be also done off-line by post-processing the thermal signal [7]. Most of the studies employ a low-frequency cyclic excitation (tens of Hertz) so that the response of the specimen is not amplified by resonance, but fast enough to meet adiabatic conditions.

Under the increasing popularity of non-invasive optical techniques in experimental mechanics and, specifically, for experimental vibration and modal analysis [8], TSA methodology can be also exploited for this purpose. These techniques, such as Digital Image Correlation, Laser Vibrometry or Electronic Speckle Pattern Interferometry, provide full-field measurement with a very high spatial density of measurement points and eluding mass-loading effect that alters the real behaviour of the specimen under test [9–13]. Mode shapes or deformations for specific resonances take advantage of the dense meshes and, hence, it is a powerful tool to validate theoretical and numerical models. However, strain fields are obtained by post-processing. Specifically by computing spatial derivatives that yields a quite significant increment of the spatial noise in the resulting strain field. Conversely, the analysis of temperature variation can provide

modal features related to stress/strain fields without post-processing, which might also provide complementary information to current full-field displacement techniques.

As reported in previous works, one of the main concern in dynamic events with vision techniques is, besides the frame rate, the shutter or exposure time. The motion is observed as a variation of the pixel intensity due to the position change of the object within the field-of-view of the camera [14]. Hence, the shutter must be fast enough to minimise the blurring due to the fast motion of the specimen during the exposure of the camera sensor. In vibration analysis, it must be shorter than the period of the vibration to discretise the cycle properly. However, excessively short exposure time produces dark and low contrast images that will be hard to be processed.

For IR camera, the shutter analogous parameter is the integration time. During it, the sensor is receiving IR radiation. In this case, the pixel is intended to represent a unique point of the specimen to obtain its temperature variation over time. Therefore, a short integration time just makes it difficult to register low temperatures due to low radiation. Long integration time produces the same effect than long exposure time in vibration. This is therefore the main parameter to fix for IR cameras in order to register high-frequency temperature oscillations in ambient conditions.

Some studies provide preliminary results of the investigation of thermography for modal parameter determination. Natural frequency detection was performed in a plate by inspecting the temperature signal in the frequency domain using a white noise excitation, but no mode shape was provided [15]. Normalised stress fields associated with mode shapes were analysed in other works. However, some of them provide no information about the relevant recording parameters [16,17]. In addition, either no validation was performed or not clear conclusions can be made from it. Backman and Greene [18] remarked the importance of the integration time, suggesting a third of the vibration period for adequate sampling. Their work provides shapes of hundreds of Hertz of a gas turbine blade and one high-frequency mode of 3400 Hz. However, significant information is not reported, such as the frame rate and the number of images. Very long sequences in time were recorded, up to 30 min for the 3400 Hz mode, which is a drawback that can be improved choosing a suitable number of images and frame rate. Despite the good appearance of the results, no validation was performed and the sources of noise were not deeply analysed. A deeper analysis is shown by Phan et al. [19] who present a theoretical, numerical, experimental study of beams and plate vibration. The study shows how thermal conductivity affects the measurement in metallic materials,

especially for the lowest mode (the slowest heat generation, below 20 Hz) where the correlation with the theoretical and numerical models failed. High frequencies were not investigated and thus integration time was not discussed. Additional aspects in this study can be improved, like the setup for the plate analysis, where the camera was not perpendicular to the plate due to difficulties in the setup; also the use of a unique frame rate, which is not optimal for all the modes.

The purpose of the present study is to evaluate the capabilities of thermography to obtain temperature/stress fields of mode shapes by thermoelastic effect using a modern IR camera and minutely report the parameters required for successful experimentation. Different modes of an aluminium plate are evaluated exploring up to the highest resonance measurable. The experimental methodology is thoroughly described with emphasis on the use of the appropriate integration time according to the excitation frequency. Temperature image sequences are analysed through Discrete Fourier Transform to extract the signal at the target frequency and remove the noise. Further capabilities of the IR cameras are demonstrated beyond the traditional low-frequency fatigue analysis, after observing modes over 2000 Hz for the current case. The effect of the increasing frequency on the thermal signal is illustrated and compared with the effect on displacements, where the drop of the amplitude is one of the main limitations for full-field displacement techniques [20]. The effect of the integration time was illustrated through the signal noise floor. Finally, a Finite Element (FE) analysis of the first stress invariant of the modes is provided to numerically correlate the thermal fields and evince the noise influence on the quality of the results.

2. Thermoelasticity fundamentals

Thermoelasticity is the science which studies the temperature changes associated with the elastic deformation of a solid [21]. It is based on the assumption that the body behaves elastically, and consequently, it is possible to employ the concept of reversibility of its transformations. In that case, the path leading from the initial to the final state of the system can be considered as a succession of infinite quasi-static steps. Consequently, this reversible process can be studied thermodynamically for the quasi-static states, where the internal energy and the entropy can be described as state functions [3]. Moreover, the relation between the mechanical and the thermal behaviour can be described by designating the strain tensor and the temperature as state variables. In the process to obtain the equation describing the changes in temperature induced in a body due to the thermoelastic effect, it is assumed that heat conduction between

parts of the body occurs so slowly that the phenomenon meets adiabatic conditions. Hence, the classical theory of thermoelasticity states that the application of a load in a solid produces temperature changes, ΔT, which are proportional to the variation in the sum of the principal stresses, $\Delta\sigma_{kk}$, according to the following expression [22]:

$$\Delta T = -T_0 K \Delta\sigma_{kk} = -T_0 \frac{\alpha}{\rho c_p} \Delta\sigma_{kk} \quad (1)$$

Where T_0 [K] is the temperature at the unloaded stated and K [Pa^{-1}] is the thermoelastic constant, that depends on the coefficient of thermal expansion, α [K^{-1}], the density, ρ [kg m^{-3}], and the heat capacity at constant pressure, c_P [J kg^{-1} K^{-1}], of the material. As the temperature generate infrared radiation, IR cameras, with a sensor sensitive to infrared waves, are employed to register this emission. Hence, thermoelastic stress analysis provides full-field stress maps by measuring temperature changes in a non-invasive way. The order of the temperature variations is mK so, generally, variation in thermal images is highly polluted by noise. Traditionally, cyclic excitation (with a frequency high enough to achieve adiabatic conditions) has been employed as an efficient way to reject noise since the response at the frequency excitation can be easily filtered out using a lock-in amplifier or a post-processing strategy like frequency analysis. The thermoelastic information obtained is a vector whose modulus denotes the magnitude of the temperature variation and the phase the phase shift regarding the load signal. Therefore, in the case of exciting cyclically a natural frequency, the sum of normal stresses corresponding to the mode shape at that frequency can be obtained using these procedures [19].

3. Methodology

To evaluate the capability of thermography for vibration shape analysis, a laboratory study was performed on an aluminium plate of 149 x 149 mm and 2 mm thick. The plate was rigidly attached through one of its edges to a shaker, model Data Physics GW-V55/PA300E, in a vertical position using a clamping device with three M8 screws. The free surface to vibrate was finally 129 x 149 mm. To insulate thermally the plate from the clamping device, 2 mm thick polycarbonate blocks were employed at both sides. According to the phases of this study, the plate was excited by the shaker using different signals. For the different tasks of signal generation and measurement during all the experimental campaign, a vibration controller was employed, model Spider 80X. In the next subsections, specific details of the methodology are provided for every stage of the analysis here performed.

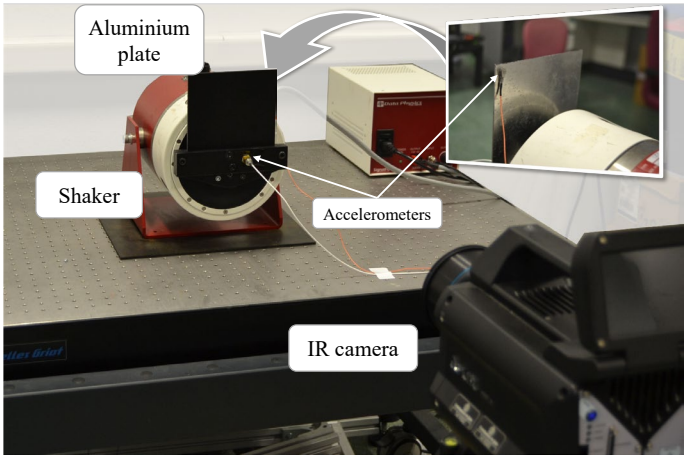

Fig. 1. Experimental setup to measure temperature with an IR camera of an aluminium plate under vibration load.

3.1. Finite Element analysis

The objective of the FE numerical analysis was the validation of the experimental results, especially as frequency increases. This numerical model was performed in ABAQUS software reproducing the experimental conditions. Only the free surface of the plate was modelled and the lower edge was fully constrained to simulate the fixation. Standard aluminium mechanical properties were employed: density of 2700 kg m^{-3}, Young's modulus of 68 GPa and Poisson's ratio of 0.3.

For the mesh, 4-nodes reduced integration shell elements (S4R) were employed. A homogeneous structured mesh was obtained with 65 x 75 elements of approximate 2 mm side, as seen in Fig. 2. The modal parameters were obtained solving the undamped eigenvalue problem using the Lanczos solver. From the result, those modes that correspond with the experimental ones were selected and, particularly, the first stress invariant at the Gauss points was taken for the later validation of the temperature maps.

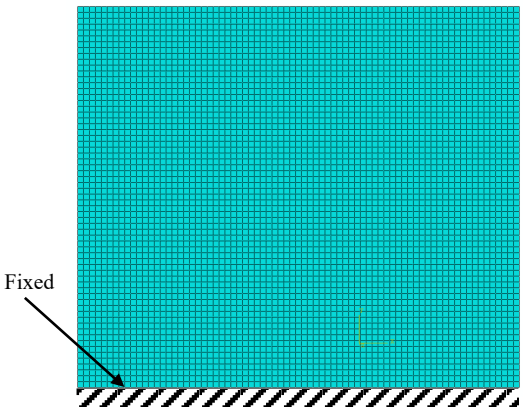

Fig. 2. FE model of the aluminium plate.

3.2. Experimental resonance identification

The first step in the experimental procedure was to identify different natural frequencies to be afterwards excited and recorded by the IR camera. For the execution of this analysis, two accelerometers were employed to estimate the frequency response function at one point of the plate from which to identify resonance peaks. One accelerometer was placed in the shaker's armature to register the excitation whereas the response was measured by another at the upper right corner. That point was supposed to be a high amplitude response point for most of the resonances and, consequently, quite appropriate to detect them. The accelerometer employed here was a Miniature Deltatron Type 4517 of Brüel & Kjaer whose weight is 0.6 g, very light, not adding significant mass to the plate. Nonetheless, after the identification, this accelerometer was not removed to maintain the conditions throughout the study. In order not to interfere with the thermal measurement, this accelerometer was placed on the back of the plate, as shown in Fig. 1.

The response of the plate up to 3500 Hz was obtained using a white noise random signal. The frequency response function was obtained using 30 averaged samples of 7200 lines, the frequency resolution of 0.625 Hz and a Hanning window. The employed resonances in this study are listed in Table 1.

3.3. Modal thermal fields measurement

Once the natural frequencies of the plate were detected in that frequency band, the specimen was excited at these frequencies using sinusoidal excitation to measure the thermal emission. The thermal signal depends on the magnitude of stresses and, hence, on the magnitude of deflection. To ensure suitable thermal signal, the excitation level in terms of acceleration was 100 m s^{-2}, according to the shaker's capability. A lower level of 20 m s^{-2} for the first mode and 70 m s^{-2} for the second to the fourth mode were employed as they generate large enough deflection.

IR emission measurement is very sensitive to the environment and the thermal properties of the material. Aluminium reflects easily the radiation and may produce misleading results. Therefore, the plate was painted with a black matt paint to enhance the emissivity and avoid reflections. For the same purpose, the clamp was also painted. In this way, the recorded signal is just a consequence of the thermoelastic effect.

An IR camera model FLIR X6581sc was employed with a 50 mm focal length lens that allows a view angle of 11° x 8.8°. It was placed perpendicular to the plate, as shown in Fig. 1. The sensor type is a digital focal plane array made of indium antimonide (InSb) and cooled with a closed-cycle Stirling cooler. This model

is able to capture about 303 fps at full resolution, 640 x 512 pixels, and operates in the spectral range between 1.5-5.5 μm. In these tests, the maximum resolution was achieved by fitting the plate within the field of view.

As previously stated, when high-frequency vibrations are recorded, two parameters are determinant: frame rate and integration time. Despite the natural frequencies were higher than the available frame rate, this issue is easy to overcome using a subsampling strategy. Actually, it is observed that only the first mode might fulfil the Nyquist criterion according to the camera's maximum frame rate. The criterion in this study is to choose the frame rate for every resonance in such a way to get a cycle characterised by many points (>10 points per cycle), so the frame rate must be much higher than the frequency of interest. Therefore, the frame rate was chosen so that the alias frequency fulfils that condition, i.e., the closest multiple of the frame rate to the excitation frequency must be as close as possible to the excitation frequency itself. As seen in Table 1, all the modes were eventually subsampled with the specified frame rate. The resulting alias frequency is also provided as that difference. As a result, the information contained in the images sequence is maximised. However, the images sequence still needed to be long due to the low level of the signal: 5 000 frames composed the sequences for the first two modes and 10 000 frames for the rest, but recording time was always inferior to 1 minute, as can be deduced.

The integration time is the real limitation for this analysis since it should be many times shorter than the vibration period. However, during a very short integration time, a very low level of IR radiation is received by the camera sensor for ambient conditions and the temperature signal is polluted by noise. Therefore, in order to explore the capabilities of this technology, the criterion to assign the integration time for each resonance was a maximum time of 30-40% of the vibration period [18]. Table 1 also includes the employed value of this parameter for every mode.

Table 1. List of the analysed resonances and the corresponding IR camera recording parameters employed in each test.

Mode	Natural frequency (Hz)	Integration time (μs)	Frame rate (fps)	Alias frequency (Hz)
1	108	1000	100	8
2	206	800	200	6
3	560	600	284	8
4	614	500	206	4
5	788	400	260	8
6	1276	310	254	6
7	1419	210	285	6

8	1846	180	265	9
9	2128	170	265	8
10	2427	130	269	6
11	2708	110	300	8

3.4. Data processing

The images sequences obtained as described above represents the absolute temperature of the plate over time, which contain constant frequency sinusoidal oscillation at the test frequency. To extract and process the contained data in these sequences, the images were handled with Python code. The temperature signal over time for each pixel was transformed into the frequency domain using a Discrete Fourier Transform routine. Then, the temperature map corresponding to the vibration frequency, equivalent to the first stress invariant, was obtained by showing an image of the amplitudes of the precise frequency line.

For the comparison with FE, the thermal map corresponding to each resonance was resized to fit the FE mesh (65 x 75 elements). The correlation coefficient of the equivalent resonances was then calculated to provide a quantification of the comparative.

4. Results and discussions

As a result of the described methodology, two sets of maps were obtained. First, the experimental procedure provides the temperature maps of the indicated resonances, proportional to the first stress invariant. Modes 1-6 are shown in Fig. 3 and modes 7-11 in Fig. 5. The second set represents the normalised first stress invariant maps of such resonances obtained numerically with FE, as shown in Fig. 4 and Fig. 6 for modes 1-6 and 7-11, respectively. Figures are presented alternatively to facilitate the comparison of both methods. As an underdetermined eigenproblem, mode shapes are usually normalised. However, the experimental images are shown as the temperature real magnitude to show the level of the signal.

In the first-sight comparison of equivalent modes, the figures illustrate the capability of this technology for the evaluation of first stress invariant of mode shapes in a wide range of frequencies. The experimental analysis returned very detailed full-field temperature maps. The quality falls gradually as the frequency of the modes increases because the shaker motion in terms of displacement decreases with squared frequency for constant acceleration, as performed in this study. Fig. 7 shows the correlation coefficient between both techniques for every mode. The trend of the correlation confirms this quantitatively. Two factors take part:

first, the level of displacements decreases with higher frequencies and so does the stress, therefore the level of the IR radiation also falls; and second, lower integration time is required which makes noise rise. The combination of both factors makes the signal-to-noise ratio fall. The most evident increment of noise in the images occurs in the 8th mode (1846 Hz). Lower modes provided clear maps and the correlation coefficients are good, over 0.85. From this mode on, the noise is more evident (the temperature oscillation is only a few mK) and the correlation coefficient starts to fall, showing a strong decreasing for the last mode (2708 Hz) with a value of 0.491. Despite that, values around 0.8 for the 9th (2128 Hz) and 10th (2427 Hz) mode are still acceptable, especially considering that they are resonances over 2000 Hz, a trend is still visible in the thermal field of the last mode in comparison with the simulation.

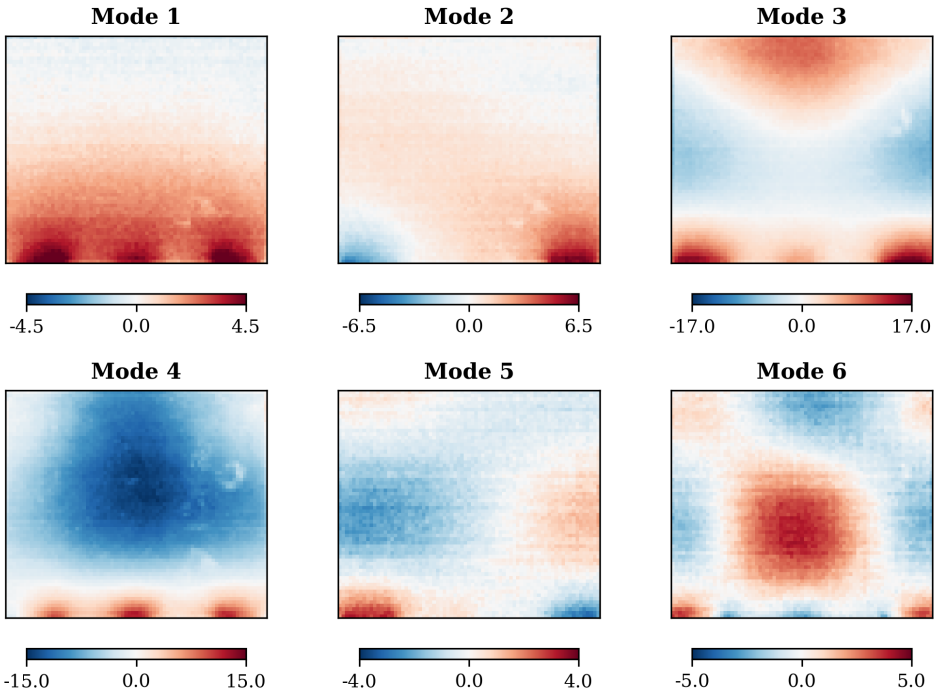

Fig. 3. Experimental temperature field (mK) corresponding to 1-6 mode shapes of the plate using the IR camera.

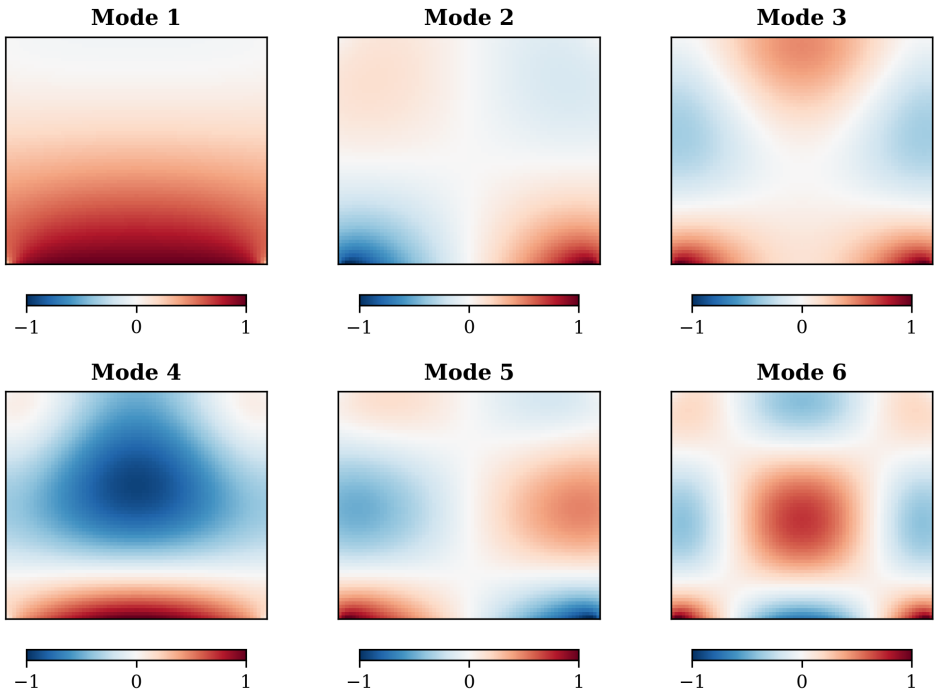

Fig. 4. Normalised first stress invariant corresponding to 1-6 mode shapes from the FE simulation of the plate.

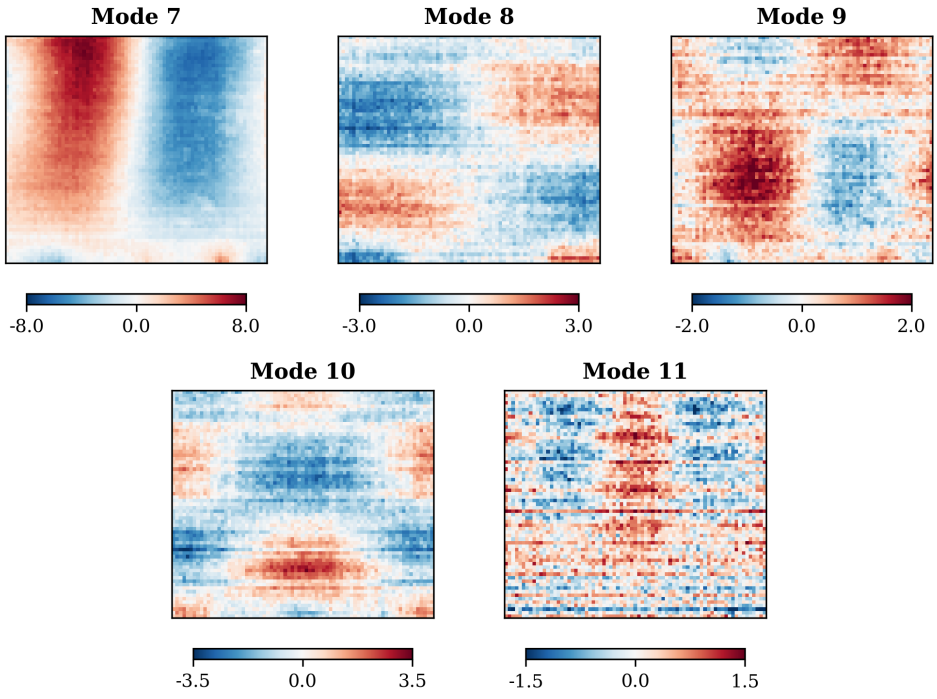

Fig. 5. Experimental temperature field (mK) corresponding to 7-11 mode shapes of the plate using the IR camera.

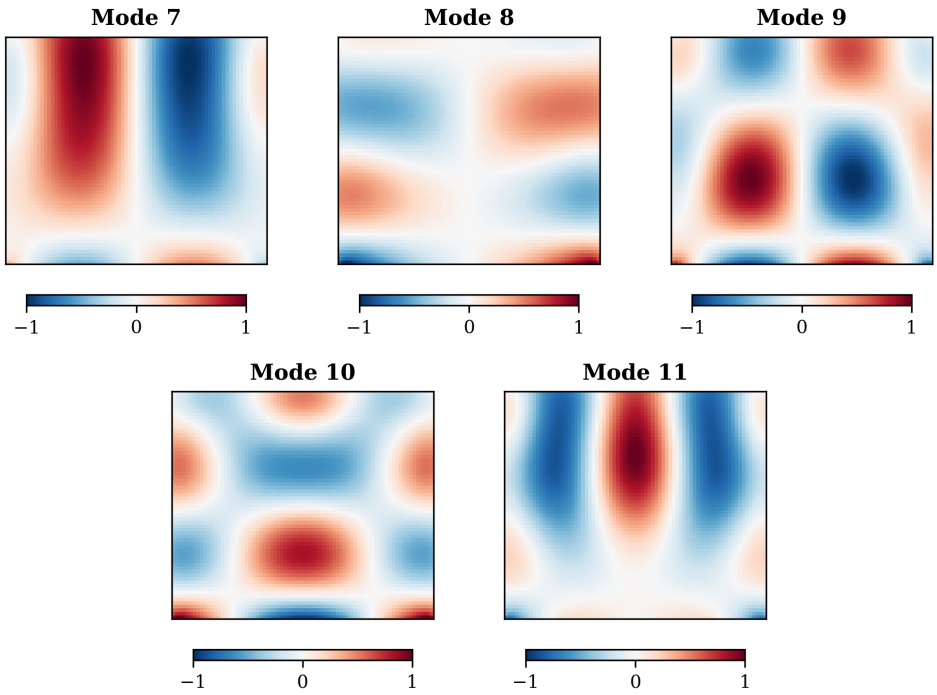

Fig. 6. Normalised first stress invariant corresponding to 7-11 mode shapes from the FE simulation of the plate.

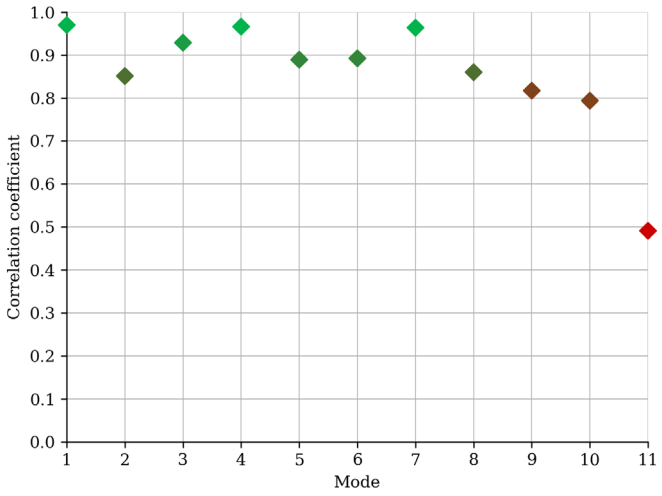

Fig. 7. Correlation coefficient of the temperature/stress maps between experimental and FE results.

Nevertheless, some factors may counteract this trend. First, it must be taken into account that the response of every mode to the applied excitation varies. It does not follow a predictable trend from one mode to another, and a full experimental modal analysis would have to be performed to determine it. However, another interesting variable influences this thermal measurement which is not present in techniques based on measuring displacement. Along with the displacement decreasing with frequency, it has to be consider

that stress fields depend on those displacement fields derivative, according to the constitutive law. It can be found that stiffness increases with modes order. That means that the deformation gradient and, thus, stress become higher for a certain deflection amplitude. To illustrate that, the ratio of each mode between the maximum value of the first stress invariant, σ_{max}, and the maximum displacement, d_{max}, from the simulation fields versus frequency is shown in Fig. 8a. However, the displacement amplitude decreases exponentially with squared frequency for a given acceleration. If this effect on the plate stresses is evaluated, without considering the frequency response, it will be equivalent to calculate this ratio in terms of the maximum acceleration in the plate, a_{max}, depicted in Fig. 8b. The dashed line represents the hypothetical case where the relation between stress and deflection was the same for all the modes, taking the amplitude of the first mode as a reference, i.e, a flat line in Fig. 8a. This curve is then equivalent to the displacement reduction. Fig. 8b shows how the reduction in displacements is more pronounced than in stresses, therefore, the increment of the mode stiffness attenuates it. Then, the frequency response of each mode is superimposed on it, but, as observed for this plate, the difference of the magnitude of stress between modes in the analysed spectrum is of the order of 10^1, whereas it would be 10^2 for displacement measurement. This difference may be absorbed by common variations between modes response, yielding certain modes with higher thermal signal than inferior order modes.

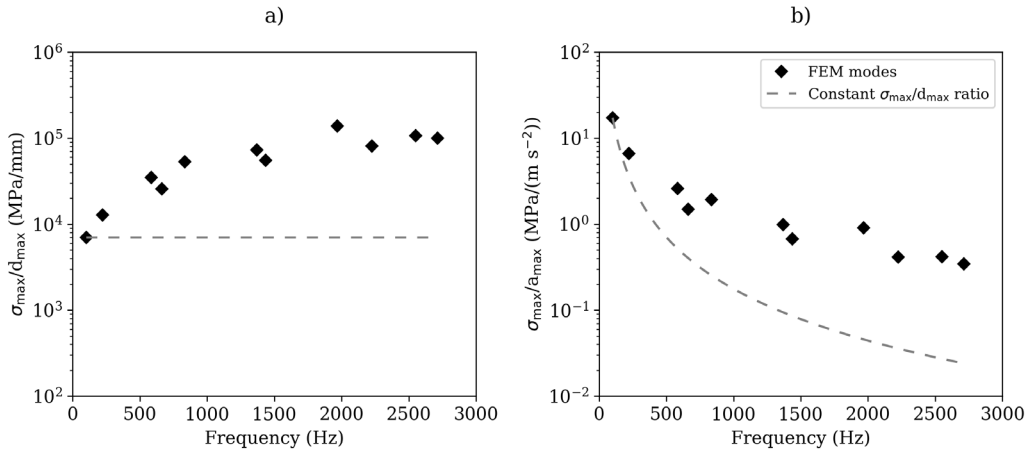

Fig. 8. Ratio between the maximum value of the first stress invariant and the maximum amplitude of the eleven mode shapes in terms of (a) displacement and (b) acceleration from the FE data. The dashed line represents the evolution of a ratio equal to the first mode over frequency.

In these tests, one of the principal variations of the response of the plate is due to the symmetry. According to the symmetrical distribution of the load with respect to the vertical axis (motion transmitted from the lower edge with the same amplitude and phase across it), the response of those resonances whose modal shape is anti-symmetrical are harder to excite, and then, the transmission of the vibration is lower. Actually,

those modes would not be excited in ideal conditions under this load. To illustrate this, those modes excited with the same amplitude are considered. First, consider modes 2-4, which were excited at 70 m s^{-2}. It can be observed that the magnitude of the thermal signal of the second mode is significantly lower, despite being a lower order mode and the attenuation of the stresses observed in Fig. 8b. The reason is that this mode is anti-symmetrical unlike the third and the fourth, which both are symmetrical and overcome the attenuation. Considering now modes 5-11, something similar can be said to modes 5^{th}, 8^{th} and 9^{th} when compared with mode 10^{th}, for instance. However, the 7^{th} mode is an exception, as it is anti-symmetrical but the thermal field is quite clear and its magnitude is relevant. The reason is related to the boundary conditions: free-clamped horizontally and free-free vertically. This mode is a triple vertical bending and single horizontal bending, so its deformation is less restricted by the boundary conditions. Hence, inferior modes like the also anti-symmetrical 5^{th} mode or even the symmetrical 6^{th} mode experienced fewer stresses as they are double horizontal bending modes. Hence, the symmetrical 1^{st}, 3^{rd} and 4^{th} modes along with the 7^{th} showed the highest the correlation coefficients with the simulation, close to one.

To illustrate the influence of the integration time, the level of noise for the first and the last mode is discussed as they required the longest and the shortest integration time, respectively. In Fig. 9, the averaged spectrum across the whole map is shown for both modes. As can be observed in these representative cases, the background is white noise whose level can be identified and compare with the signal. There is no frequency dependency of the noise in the measurement and, thus, the equal capability to detect a temperature signal with an IR camera at these particular frequency lines.

For the first mode, using an integration time of 1000 μs, the amplitude of the noise at every frequency component is about 1 mK. In this plot, it is possible to detect a clearly predominant frequency line at 8 Hz. This represents the thermal signal at the excitation frequency as can be confirmed in the list of expected alias frequencies in Table 1. The large deformation that experiences this mode produces a signal whose average is higher than the noise floor. Therefore, a clear temperature map was obtained for this mode.

On the other hand, the last mode line shows no peak at 8 Hz, where it should according to Table 1. Instead, just the white noise profile of 4 mK level is visible. That means the amplitude of the noise is higher than the signal at this frequency line. Therefore, when extracting the map at this single line, the level of noise gives the amplitude a strong arbitrary character and that is reflected as a strong spatial noise, as observed in Fig. 5. Nevertheless, a certain coherent shape was still noticed. The rest of the modes, which employed

an intermediate integration time, show intermediate behaviours. However, some variables may affect, like the frequency span or the response of the mode with respect to the excitation.

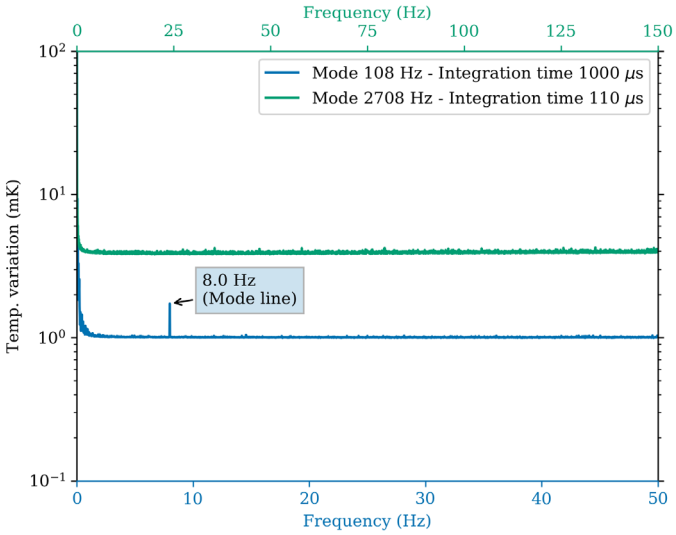

Fig. 9. Frequency domain signal obtained by the IR camera, averaged across the plate, for the first and last mode.

5. Conclusions

In this study, a thorough experimental analysis of the use of IR cameras is performed to characterise temperature oscillation of mode shapes generated by the thermoelastic effect, which is directly related to the first stress invariant. It has been shown the capability to characterise higher frequencies events than usual and take advantage of it for modal characterisation. Multiple modes with high order deformation have been characterised with great quality. Moreover, the validity of the results has been proved through the agreement with simulation stress maps and its high correlation coefficients.

Hence, the current limits of the methodology have been exposed, showing how noise affects the maps as the resonance frequency increase. It has been justified as a signal reduction because of the amplitude of deformation. Nevertheless, it has been shown that the attenuation of the thermal emission with frequency is softer than the one happening to displacements, which is the main limitation of full-field displacement techniques. Integration time also contributes to the reduction of the signal-to-noise ratio because of increasing the noise floor. Nevertheless, it is expected that it enhances in the future when more advances technologies arise with higher sensitivity IR sensors.

The experimental procedure has been accurately presented and explained to enable further experimentation. This study opens new paths in experimental modal analysis as it offers stress fields associated with mode shapes. Therefore, it would be a powerful complement for full-field displacement techniques and their recent methodologies for modal analysis, known the major importance of stresses in structural integrity.

References

[1] C. Ibarra-Castanedo, J.M. Piau, S. Guilbert, N. Avdelidis, M. Genest, A. Bendada, X.P.V. Maldague, Comparative study of active thermography techniques for the nondestructive evaluation of honeycomb structures, Res. Nondestruct. Eval. 20 (2009) 1–31. https://doi.org/10.1080/09349840802366617.

[2] V.P. Vavilov, D.D. Burleigh, Review of pulsed thermal NDT: Physical principles, theory and data processing, NDT E Int. 73 (2015) 28–52. https://doi.org/10.1016/j.ndteint.2015.03.003.

[3] G. Pitarresi, E.A. Patterson, A review of the general theory of thermoelastic stress analysis, J. Strain Anal. Eng. Des. 38 (2003) 405–417. https://doi.org/10.1243/03093240360713469.

[4] R.J. Greene, E.A. Patterson, R.E. Rowlands, Thermoelastic Stress Analysis, in: Springer Handb. Exp. Solid Mech., Springer US, Boston, MA, 2008: pp. 743–768. https://doi.org/10.1007/978-0-387-30877-7_26.

[5] R.A. Tomlinson, A.D. Nurse, E.A. Patterson, On determining stress intensity factors for mixed mode cracks from thermoelastic data, Fatigue Fract. Eng. Mater. Struct. 20 (1997) 217–226. https://doi.org/10.1111/j.1460-2695.1997.tb00279.x.

[6] T.R. Emery, J.M. Dulieu-Barton, Thermoelastic Stress Analysis of damage mechanisms in composite materials, Compos. Part A Appl. Sci. Manuf. 41 (2010) 1729–1742. https://doi.org/10.1016/j.compositesa.2009.08.015.

[7] G. Pitarresi, Lock-In Signal Post-Processing Techniques in Infra-Red Thermography for Materials Structural Evaluation, Exp. Mech. 55 (2015) 667–680. https://doi.org/10.1007/s11340-013-9827-1.

[8] J. Baqersad, P. Poozesh, C. Niezrecki, P. Avitabile, Photogrammetry and optical methods in structural dynamics – A review, Mech. Syst. Signal Process. 86 (2017) 17–34. https://doi.org/10.1016/j.ymssp.2016.02.011.

[9] Á. Molina-Viedma, E. López-Alba, L. Felipe-Sesé, F. Díaz, J. Rodríguez-Ahlquist, M. Iglesias-Vallejo, Modal Parameters Evaluation in a Full-Scale Aircraft Demonstrator under Different Environmental Conditions Using HS 3D-DIC, Materials (Basel). 11 (2018) 230. https://doi.org/10.3390/ma11020230.

[10] R. Huňady, P. Pavelka, P. Lengvarský, Vibration and modal analysis of a rotating disc using high-speed 3D digital image correlation, Mech. Syst. Signal Process. 121 (2019) 201–214. https://doi.org/10.1016/j.ymssp.2018.11.024.

[11] Y.-H. Chang, W. Wang, J.-Y. Chang, J.E. Mottershead, Compressed sensing for OMA using full-field vibration images, Mech. Syst. Signal Process. 129 (2019) 394–406. https://doi.org/10.1016/j.ymssp.2019.04.031.

[12] A. Zanarini, Competing optical instruments for the estimation of Full Field FRFs, Measurement. 140 (2019) 100–119. https://doi.org/10.1016/j.measurement.2018.12.017.

[13] Á.J. Molina-Viedma, L. Felipe-Sesé, E. López-Alba, F.A. Díaz, Comparative of conventional and alternative Digital Image Correlation techniques for 3D modal characterisation, Measurement. 151 (2020) 107101. https://doi.org/10.1016/j.measurement.2019.107101.

[14] H. Schreier, J.-J. Orteu, M.A. Sutton, Image Correlation for Shape, Motion and Deformation Measurements, Springer US, Boston, MA, 2009. https://doi.org/10.1007/978-0-387-78747-3.

[15] Z. Stankovičová, V. Dekýš, P. Novák, B. Strnadel, Detection of Natural Frequencies Using IR Camera, Procedia Eng. 192 (2017) 830–833. https://doi.org/10.1016/j.proeng.2017.06.143.

[16] A. Di Renzo, R. Marsili, M. Martarelli, M. Moretti, G. Rosati, G.L. Rossi, Simultaneous application of scanning laser vibrometry and thermoelasticity for measurement of stress-strain fields on mechanical components, in: Seventh Int. Conf. Vib. Meas. by Laser Tech. Adv. Appl., Ancona, 2006: p. 63450H. https://doi.org/10.1117/12.693161.

[17] R.K. Fruehmann, J.M. Dulieu-Barton, S. Quinn, J. Peton-Walter, P.A.N. Mousty, The application of thermoelastic stress analysis to full-scale aerospace structures, J. Phys. Conf. Ser. 382 (2012) 012058. https://doi.org/10.1088/1742-6596/382/1/012058.

[18] D. Backman, R.J. Greene, Gas turbine blade stress analysis and mode shape determination using thermoelastic methods, Appl. Mech. Mater. 13–14 (2008) 281–287. https://doi.org/10.4028/www.scientific.net/AMM.13-14.281.

[19] T.S. Phan, J.M. Dulieu-Barton, P. Temarel, Thermoelastic Stress Analysis of Structures Under Natural Vibrations, Exp. Mech. 46 (2006) 463–472. https://doi.org/10.1007/s11340-006-8445-6.

[20] A.J. Molina-Viedma, L. Felipe-Sesé, E. López-Alba, F. Díaz, High frequency mode shapes characterisation using Digital Image Correlation and phase-based motion magnification, Mech. Syst. Signal Process. 102 (2018) 245–261. https://doi.org/10.1016/j.ymssp.2017.09.019.

[21] W. Nowacki, Thermoelasticity, 2nd ed., Pergamon, 1986. https://doi.org/10.1016/C2013-0-03247-1.

[22] W. Thomson, II. On the thermoelastic, thermomagnetic, and pyroelectric properties of matter, London, Edinburgh, Dublin Philos. Mag. J. Sci. 5 (1878) 4–27. https://doi.org/10.1080/14786447808639378.